AIRFLOW IN MULTI-AIR DUCTS OF SEMICONDUCTIVE THERMOELECTRIC HEAT PUMPS

Fuyun Zhao, PhD., College of Civil Engineering, Hunan University,
Guangfa Tang, Professor, College of Civil Engineering, Hunan University,
Di Liu, Mrs., College of Civil Engineering, Hunan University,
Zhiqiang Liu, PhD., School of Energy and Power Engineering, Central South University,
Changsha, Hunan, China

ABSTRACT

This paper reviews the history and advantages of semi-conductive thermoelectric heat pumps and natural convection in vertical channels, sets up physical and numerical models of one semi-conductive refrigerator , and analyzes configurations of its multi-air ducts. Outer air is introduced into the bottom entrance of heating channel and the top entrance of refrigerating channel, and suitable boundary conditions are set up. All the numerical simulations are dominated by the following parameters, Rayleigh number (10^3-10^7), refrigeration coefficient C_{OR} (0.1-10.0), the relative conductivity ratio of walls A_W (0.1-10.0), and other thermo-physical constants and geometric parameters, such as Prandtl number and ratio of thick wall *t/h*, etc. Tables and figures present numerical results from analyzing airflow and conjugating heat-transfer characteristics of heating and refrigerating channels. There is discrepancy between the heating and refrigerating channels because of buoyancy/gravitation direction; the conductivity ratio of walls also significantly affects the flow and heat transfer along with varied *Ra* and C_{OR}. The findings could be applied to the experimental process and optimized by simulation.

Keywords: ***thermoelectric heat pump, multi-air duct, conjugate heat transfer.***

Nomenclature

b	width of single channel (m)	**Greek Symbols**	
C_{OR}	refrigeration coefficient	λ	thermal conductivity (m/s^2)
Gr	Grashof number, $g\beta_f\triangle Th^3/\nu_f^2$	β	coefficient of thermal expansion (K^{-1})
h	height of thermoelectric pairs (m)	θ	dimensionless temperature
L	height of vertical channels (m)	ν	kinematics viscosity (m^2/s)
M	Mass flow rate (m^2/s)	ρ	density of fluid (kg/m^3)
$\overline{Nu}$, Nu_l	average and local Nusselt number	α	thermal diffusivity (m^2/s)
Pr	Prandtl number, ν/α	ψ	stream function (m^2/s)
q	heat flux of volumetric heat source (W/m^3)		
Ra	Rayleigh number, $g\beta_f\triangle Th^3/\nu_f\alpha_f$	**Subscripts**	

S	area of heat source (m^2)	i	different materials/zones
T	dimensional temperature (K)	f	values of the fluid
u, v, U, V	Velocity components in x, y (X, Y) directions	C, H, R	values on the components, heaters and refrigerators respectively
x, y, X, Y	Cartesian coordinates	J	Joule heating or electric power

1 INTRODUCTION

The interaction between the thermal and electric phenomena (Joule effect, Seebeck effect, Peltier effect and Thomson effect) are known since the 19th century, and already in 1885 the English physicist J.W. Rayleigh outlined the possibility of using thermoelectric devices as electricity generators, even though this development was totally stopped because of the low efficiency achieved (Rowe and Bhandari 1983). The main advance was produced when semiconductors were incorporated in the thermoelectricity. It was observed that they had a high Seebeck coefficient, good electrical conductivity and low thermal conductivity, in other words, a higher number in the figure of merit "Z" (a dimensional number that connects these three parameters). In those moments, thermoelectric refrigeration applications were developed with Peltier devices, although most of these applications were for the military field. Nowadays, in the civil market, the thermoelectric refrigeration has a place in medical applications and scientific mechanisms and devices for which accurate temperature control is necessary. Nevertheless, there are other applications with great potential that are beginning to generate interest within manufacturers of, for instance, dehumidifiers (Vian et al. 2002), domestic air-conditioning systems, or automobiles, portable iceboxes, domestic refrigerators, transport of perishable products, dealer machines, foods expositors etc., in which this technology must compete with vapor-compression refrigeration systems. If you consider the global environment and energy emergencies, the thermoelectric refrigerator/heater remains an attractive option—it has no moving parts, is not noisy, does not vibrate, , is dependable , convenient to maintain, long-lived, and can use waste heat, such as disposed or remained heat source. Esartea et al. (2001) have modeled heat exchangers for thermoelectric generators, including spiral, zig-zag and straight fins, and analyzed the influence of fluid flow rate, heat exchanger geometry, fluid properties and inlet temperatures on the power supplied by the thermoelectric generator, and given an easy and compact expression for temperature difference of supplied Peltier module. Suzuki and Tanaka (2003) have mathematically simulated the thermoelectric power generation with the multi-panels exposed to two thermal fluids, and found that the multiplication of thermoelectric panels can shorten significantly the device area, although the output from the multi-panels decreases a few percent. Astrain et al. (2003) presented out a device for the dissipation the heat from the hot side of Peltier pellets in thermoelectric refrigeration by optimizing the complex construction. All these are limited to analyze the heat dissipation of the heating side, and lack of systematic analysis and details of these affecting factors.

The natural convection cooling problem for electronic equipment with thermal sources is a very common and desirable method for removing heat from the equipment. The application of natural

convection cooling for electronic equipment ranges from individual transistors to mainframe computers and from power supplies to telephone switchboards. Renewed interest in laminar natural convection in vertical channels stems from increasing applications in the cooling of electronic circuit boards. Most of the past work reported in the literature concerns removing heat from heating components. The interacting natural convections between two separated heated vertical plates analyzed by Sparrow and Faghri (1980), and the local and average heat transfer rates on the upper plate were numerically determined. The parallel heated plates were also analyzed by Kim et al. (1991), and the boundary layer with asymmetric heating conditions and channels subjected to repeated boundary conditions were discussed by Kim et al. (1991); The vertical channels with single surface mounted heat-flux module and with discretely heated plates were investigated by Desrayaud and Fichera (2003) and Manca et al. (2002) respectively; And the effects of outside free convection and axial conduction on forced convection heat transfer inside a cooling/heating vertical channel were investigated by Chow et al. (1984). Said and Krane (1990) performed a numerical and experimental investigation of natural convection in an isothermal channel with a single rounded obstacle. While these studies all dedicated to the heat removing of heated source. In fact, many semiconductors are fixed on the circuit boards or the vertical plates, and then thermoelectric effects of semiconductors on the circuit boards or the vertical plates were ignored. In this paper, the refrigeration/heating of components will be analyzed together.

Natural convection between series of vertical parallel plates with embedded refrigerator and heater pairs is considered in this paper to model above real cases. A schematic of a series of channels, with b_H width in heating channels and b_R width in cooling or refrigerating channels, considered for the purpose of the present analysis is shown in Fig.1. Heater/refrigerator pairs, with the same dimensions ($t/2\times h$), are centered on the vertical plates, and the repeated boundary conditions are employed on the series. The first and the last channel, however, are subjected to different boundary conditions . At first step, attention is focused on channel walls with flush-mounted, plane heat sources but without considering the support shelves. It should be noted that the simulated heat source is manifested as a plane source and then consideration is given only to two-dimensional free convective flow in this work. And the disturbance between inlet and outlet for heating or cooling channels is ignored. The airflow conditions that exist in the middle channels are the same and a computational domain can be isolated as shown in Fig. 1, and it will not like that of Kim et al. (1991), considering the numbers of planes. And the periodic or repeated boundary conditions will be addressed. As shown in Fig. 1, the width of domain W, ($W=b_H+2t+b_R$), and the periodic boundaries will be employed on the two solid sides. In the following sections, model development, solution technique, validation of the solution, and the discussion of varied results will be presented.

2 MATHEMATICAL FORMULATIONS AND NUMERICAL SOLUTION

For the heater/refrigerator pairs, the heat flux flow direction is followed the second law for thermodynamics. That is to say, the heat flux flowing into refrigerator side plus the Joule heat generated

by thermoelectric force or the electric power equals the heat flux dissipated from the heater, and the thermal balance is written as (the geometric sizes of heater is same as that of refrigerator):

$$q_R + q_J = q_H \tag{1}$$

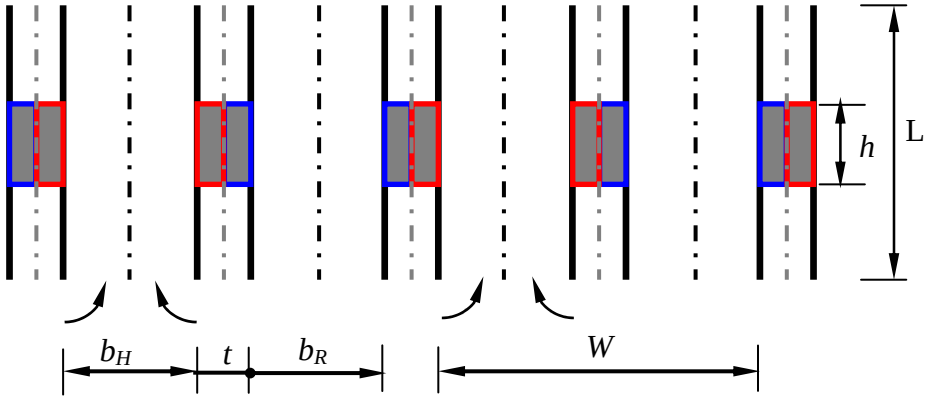

Fig. 1. Schematic of series of channels (red and blue frames denote Heaters/Refrigerators respectively.)

And the refrigeration coefficient Co_R is defined as q_R/q_J, and the equation (1) turns into, $C_{OR} + 1 = C_{oH}$, where the C_{oH} is heating coefficient. In this paper, the detailed characteristics of P-type and N-type elements or that of heat pumps will not be discussed, and the semiconductors will be assumed as one heater and one refrigerator, all thermo/magnetic effects other than Joule effect are ignored, and the equation (1) is the sole one of thermoelectric effects. Assuming a steady state, laminar flow with negligible viscous dissipation and pressure stress terms, the full elliptic equations governing the flow are solved numerically using the control volume method under the Boussinesq-fluid assumption. The dimensionless equations are written in strong conservative form,

$$\frac{\partial U}{\partial X} + \frac{\partial V}{\partial Y} = 0 \tag{2}$$

$$\frac{\partial UU}{\partial X} + \frac{\partial VU}{\partial Y} + KU = -\frac{\partial P}{\partial X} + \sqrt{\frac{\Pr}{Ra}}\left(\frac{\partial^2 U}{\partial X^2} + \frac{\partial^2 U}{\partial Y^2}\right) \tag{3}$$

$$\frac{\partial UV}{\partial X} + \frac{\partial VV}{\partial Y} + KV = -\frac{\partial P}{\partial Y} + \sqrt{\frac{\Pr}{Ra}}\left(\frac{\partial^2 V}{\partial X^2} + \frac{\partial^2 V}{\partial Y^2}\right) + \theta \tag{4}$$

$$\frac{\partial U\theta}{\partial X} + \frac{\partial V\theta}{\partial Y} = A_i\sqrt{\frac{1}{\Pr Ra}}\left(\frac{\partial^2 \theta}{\partial X^2} + \frac{\partial^2 \theta}{\partial Y^2}\right) + \begin{Bmatrix} 0 \\ (1+Co_R)A_C\sqrt{\frac{1}{\Pr Ra}} \\ -Co_R A_C\sqrt{\frac{1}{\Pr Ra}} \\ 0 \end{Bmatrix} \tag{5}$$

Then the conjugate heat transfer could be solved together. And in Equation (5), the A_i denotes the ratio of thermal conductivities, the footnote *i* represents different zones or materials, 1, $\frac{\lambda_C}{\lambda_f}$, $\frac{\lambda_C}{\lambda_f}$ (i.e. A_C), and $\frac{\lambda_W}{\lambda_f}$ (i.e. A_W) are set for fluid, heater, refrigerator and thick walls respectively. Commonly, the semiconductor is made of silicon or its components, and the thermo-physical parameters of heater/refrigerator are constant, accordingly, the ratio A_C is set 5.0 for most cases in this paper (or it can be modeled as a heat pump). The geometric dimensions, velocity and temperature difference were non-dimensionalized by *h*, $\sqrt{g\beta_f \Delta Th}$, and $\Delta T = \frac{q_J h^2}{\lambda_f}$. The solid and fluid parts are taken into account through the use of the purely numerical K-parameter, K equals infinite for the solid parts and K equals zero for the fluid parts. The governing parameters Rayleigh number (*Ra*) and the Prandtl number (*Pr*) are expressed in nomenclature, and for the airflow cooling/heating.

Equations (2)-(5) can be numerically solved by SIMPLE algorithm (Patankar, 1980). In order to improve numerical accuracy, the third-order deferred-correction QUICK scheme (Hayase et al. 1992) and second-order Central Difference Scheme are, respectively, employed for the convection and the diffusion terms. The discretized equations are solved iteratively using the line-by-line TDMA (Tri-Diagonal Matrix Algorithm). To solve the conjugate heat transfer problem, the grid layout is such that the fluid-solid interface forms a control volume face for the neighboring grid points. The abrupt changes of thermal conductivities at the interface between the fluid and solid regions are handled by harmonic mean formulation (Patankar, 1980). The global solution procedure facilitates the code programming, making it easier to solve the conjugate heat transfer problem, regardless of increasing requirement of computational storage and time. Heat transfer local and average Nusselt numbers, dimensionless mass flow rate and stream function Ψ are defined respectively by the following expression,

$$Nu_l = \left|\frac{\partial \theta}{\partial n}\right|_{Local} \qquad \overline{Nu} = \int_l \left|\frac{\partial \theta}{\partial n}\right|_{Local} dl \qquad M = \int V dX \qquad \psi = \int -V dX + U dY$$

The footnote *Local* means any location that is normal the surface of walls. The dimensionless mass flow rate is calculated at any horizontal location *Y* in channels by the above expression, and if on the outlet or inlet location, the *U* in the above equation is,
If $V_{Y=L/h} \geqslant 0.0$, $V=V_{Y=L/h}$, and if $V_{Y=L/h}<0$, $V=0$; If $V_{Y=0} \geqslant 0.0$, $V=V_{Y=0}$, and if $V_{Y=0}<0$, $V=V_{Y=0}$.
Stream function Ψ are computed from the velocity distributions, and Ψ is zero in the integration starting point. Here should be pointed out, the central vertical hidden lines in Fig. 1 half the whole computational domain into two parts, and un-continuities of mass and energy should be encountered on the lines, and two parts should be solved separately, while the heat flux from heater to refrigerator has been

implemented by the source terms in Equation (5). The non-slip conditions are employed, then the U=V=0 is valid in solid zones. Then the following boundary conditions are applied,

X=0, *W/h* $\frac{\partial \theta}{\partial Y} = 0$, *U*=*V*=0 (insulated boundaries).

(*X*, *Y*) = ((0, b_H/*h*), 0), and (*X*, *Y*) = ((b_H+*t*)/*h*, *W*/*h*), *L*/*h*) *U*=0, $\frac{\partial V}{\partial Y} = 0$, $\theta = 0$ (Inlet boundaries)

(*X*, *Y*) = ((0, b_H/*h*), *L*/*h*), and (*X*, *Y*) = ((b_H+*t*)/*h*, *W*/*h*), 0)

$\frac{\partial U}{\partial Y}$=0, $\frac{\partial V}{\partial Y} = -\frac{\partial U}{\partial X}$, $\frac{\partial \theta}{\partial Y} = 0$ (*V*≥0) or θ=0(*V*<0) (Outlet boundaries)

X=*W*/2*h* $\left.\frac{\partial \theta}{\partial Y}\right|_{left} = \left.\frac{\partial \theta}{\partial Y}\right|_{right} = 0$, *U*=*V*=0 (inner insulated boundaries)

In order to verify the numerical methods, in Table 1, a systematic grid-independence study optimized the grid structure for computations of full heating channel in Fig. 1 is performed. After each iterated computation, the energy conservation cross the system should be verified and the general relations are expressed as,

$$\sum_i \overline{Nu_{V\,i}} = \sum_i \frac{q_i''' h^2}{\lambda_f \Delta T} \frac{S_i}{h^2} = \sqrt{Ra\,\mathrm{Pr}}\left[\int_{Outlet} V\theta dX - \int_{Inlet} V\theta dX\right] \quad (6)$$

In above equation, the $\overline{Nu_V}$ means the average Nusselt number of heat source, and the S_i denotes the area of *i*'s heat source. In Table 1, four groups of grids are used for Ra=10^5. From this table, the balances of mass flow (the flux of outlet equals the flux of inlet) and energy crossing the system (Equation 6, the total heat lost by the heat sources should be equal to the heat gained by the fluid as it flows through the channel.) are satisfied well for every group of grids, especially when denser grids being used. From the sparse grids to the densest grids, the changes of each variable's values are less than 3%, that is to say, the grid independence of this code is built up. And other cases encountered, similar ways can be used to verifying the grid independence.

Table 1. Effect of grid refinement on various local and global variables in heating channel, $Ra=10^5$, and $C_{OR}=0.0$, $A_C=A_W=1.0$, $b_H/h=2.0$, $L/h=9.0$, $t/h=0.4$

Grids	M_{Outlet}	M_{Inlet}	$\overline{Nu}_{X=t/2h}$	$\overline{Nu}_{X=W2/2h}$	$\sqrt{Ra}\,\mathrm{Pr}\int_{Outlet} V\theta dX$	$\sqrt{Ra}\,\mathrm{Pr}\int_{Inlet} V\theta dX$
41×31	0.021	0.021	0.19	0.19	0.38	0.00
81×71	0.023	0.023	0.20	0.20	0.39	0.00
121×101	0.023	0.023	0.20	0.20	0.40	0.00

3 RESULTS AND DISCUSSION

Numerical computations were performed for a range of governing parameters that may be encountered in actual applications. These input levels are collected in Table 2. The refrigeration coefficient Co_R of many refrigeration equipments ranges from less than 1.0 to higher than ten, and the listed three quantities represent most cases in application. And the materials of wall can be selected from practice, such as rubber, steel or others, and the listed ranges of A_W can cover these materials for electrical industry.

Table 2. Parametric and geometric values used in numerical computations

Parameters	Co_R	Ra	Pr	A_C	A_W	L/h	t/h	b_H/b_R	b_H/h
Values	0.1, 1.0, 10.0	10^3-10^7	0.71	5.0	1.0, 10.0, 100.0	9.0	0.4	1.0	2.0

Figure 2 shows the isotherms and streamlines for three different thermal conductivities, *Aw*=0.1, 1.0, and 10.0, denoting the insulated material and conductivity-well ones. When *Aw* equals 0.1, the heat transfer pass clustered in the vicinity of heat source, where the interface of fluid and component, whatever in heating channel or in refrigerating channel. When *Aw* increases to 1.0, the heat transfer doesn't change much, although the isotherms in refrigerating side extended to inlet (top side) a little. Correspondingly, the maximum of stream functions are little discrepancy between them. When *Aw* increases up to 10.0, and exceeds the A_C, the flow charts and isotherms change much both in heating side and refrigerating side. While, the maximum of stream function is little different from the formers in refrigerating side, and it changes a lot in heating side. These are attributed to that the heat input of heating side is higher than the heat output of cooling/refrigerating side. The variations of maximum temperature θ_{Max} and outlet mass flow rate M_{Outlet} in heating channel, and those of minimum temperature θ_{Max} and outlet mass flow rate M_{Outlet} in refrigerating channel with different *Ra* and C_{OR} numbers are depicted in Figs. 3, 4 and 5, and many interesting rules or air flow and heat transfer behaviors are investigated below.

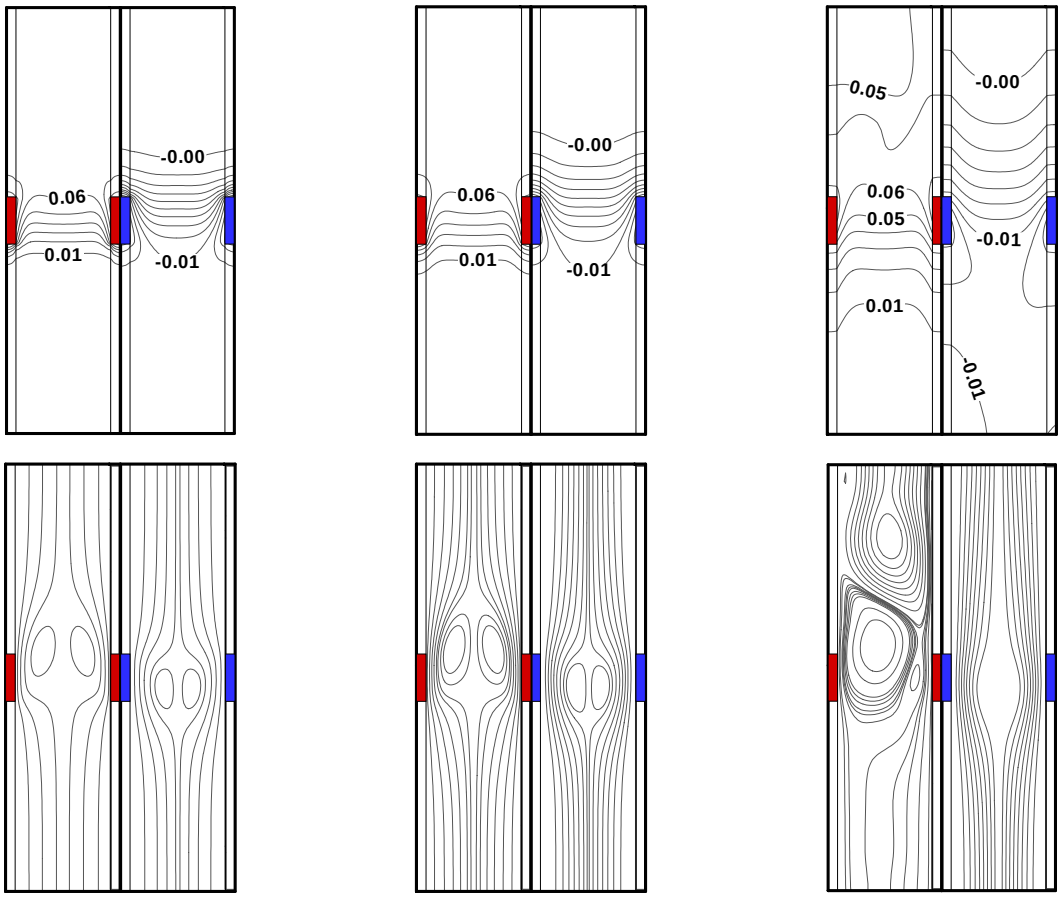

A_W=0.10 A_W=1.00 A_W=10.0

Fig. 2. Isotherms and streamlines for three thermal conductivities of wall, and *Ra*=10^5, C_{OR}=0.10

3.1 C_{OR} Equals 0.1

When C_{OR} equals 0.1, for heating channel, in 3.1 of Fig. 3, the maximum temperatures reduced with the rising of Ra numbers, which benefited for heat dissipation from heat sources when Ra number is higher. The maximum temperatures with lower *Aw* values (0.1 and 1.0) are higher than those with higher *Aw* values (10.0), and the formers are approximately when *Aw* equaled 0.1 and 1.0 respectively. These result from two sources: one, that the higher conductivity of walls can distribute the thermals more uniformly so that the maximum temperatures decrease when *Aw* ascends; the other, that the impaction of *Aw* for flow field will be neglected when it ranges little (from 0.1 to 1.0) and when *Ra* is lower. So when *Ra* exceeded 10^5, the maximum temperatures tended to consistency for Aw ranges from 0.1 to 10.0. While the outlet mass flow rates $\boldsymbol{M}_{Outlet}$ varies for different *Aw* values in 3.1 of Fig. 3. When Aw equals 10.0, the flow rates reduce along with *Ra* from 10^3 to 10^5, and rise with *Ra* from 10^5 to 10^7; when *Aw* equals 1.0, the outlet flow rates reduce along with *Ra* from 10^3 to 10^6, and increase with *Ra* from 10^6 to 10^7, while the outlet flow rates always decrease with *Ra* ranges when *Aw* equals 0.1. We can discern that the transition for the outlet flow rates moves forward with the reduction of *Aw*. These attributes to the flow transitions, from the fully developed duct flow to boundary layer flow, and the lower *Aw* retard the transition.

For the corresponding refrigerating channel, shown in 3.2 of Fig. 3, the trends of minimum temperatures along with *Ra* numbers are similar as in the heating channel when *Aw* is the same. That is to say, the absolute values of minimum temperatures reduce with the rising of Ra numbers, and the absolute values of minimum temperatures when *Aw* is higher are less than those when *Aw* is lower, although those of *Aw* equaling 0.1 are approximate to those of *Aw* equaling 1.0. These trends all result from the similar causes depicted in heating channel mentioned above. The outlet flow rates in refrigerating channel shown in Fig. 3.2 are different from the heating channel shown in Fig. 3.1. For the refrigerating channel, the sum of average Nusselt number of heat sources, $\overline{Nu_V}$, only equals 0.04, while that in heating side is up to 0.44, so the absolute minimum temperatures are much lower than the maximum temperatures when other parameters are in the same. Accordingly, the flow rates in the refrigerating channel decrease along with the increased *Ra* numbers. Here should be pointed that, when *Aw* equals 10.0, the flow rates increase firstly, and then decrease after Ra exceeding 10^5, which attributes to the flow transitions due to the uniform thermal distribution. While *Aw* is lower, the flows by two cooling sources range from the developed duct flow to regular boundary layer flow, and then the outflow rates decrease along with the increased *Ra* numbers.

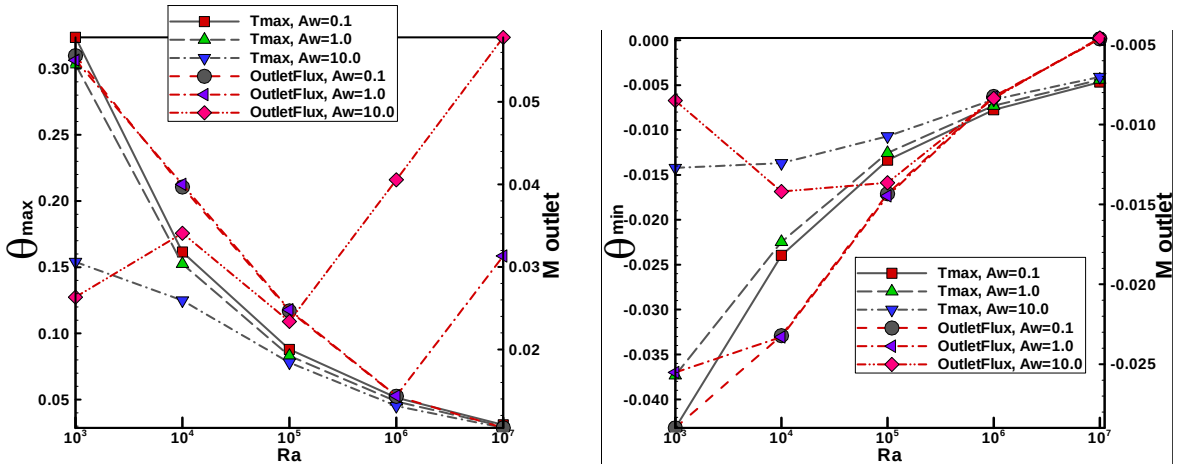

3.1 Heating channel **3.2 Refrigerating channel**

Fig. 3. Extreme temperature and mass flow rate on outlet in heating/refrigerating channels (C_{OR}=0.1)

3.2 C_{OR} Equals 1.0

When C_{OR} increases to 1.0, the sum of average Nusselt number of heat sources, equals 0.80 and 0.40 for heating and refrigerating channels respectively, therefore the heat transfer and convection in these channels will be strengthened, which can be seen from the Fig. 4.1 and Fig. 3.1, Figs. 4.2 and 3.2. In the heating channel, shown in Fig. 4.1, with the increased *Ra* and C_{OR}, the transitions of outlet flow rates are similar as above studies (Ra=10^5 for Aw=10.0, Ra=10^6 for Aw=1.0, and the transitions are not investigated for Aw=0.1 in this study). Those causes are similar with those as C_{OR} equals 0.1. The variations of

decreased maximum-temperatures along with the increased *Ra* and the varied values of Aw are similar to that of C_{OR} equaling 0.1 in the heating channel.

In the refrigerating sides, shown in Fig. 4.2, the outflow rates and the minimum temperatures are descending along the increased *Ra* numbers together, and after *Ra* exceeding 10^4, the outflow rates for different *Aw* tend to uniform, which is also encountered when C_{OR} equals 0.1 when the *Ra* amounted to 10^5 shown in Fig. 3.2. The ahead of outflow rates uniformity are induced by the increased cooling source, from 0.04 to 0.4 (also the sum of average Nusselt number of cooling sources), which insures the flow states as fully developed duct flow. While in heating channel, the sum of average Nusselt number of heating sources is higher than that in cooling sides, $\overline{Nu_V}$ equals 0.44 when C_{OR} is 0.1, and it equals 0.80 when C_{OR} is 1.0. Therefore, fully developed duct flow in heating side is destroyed and transited into boundary layer flow.

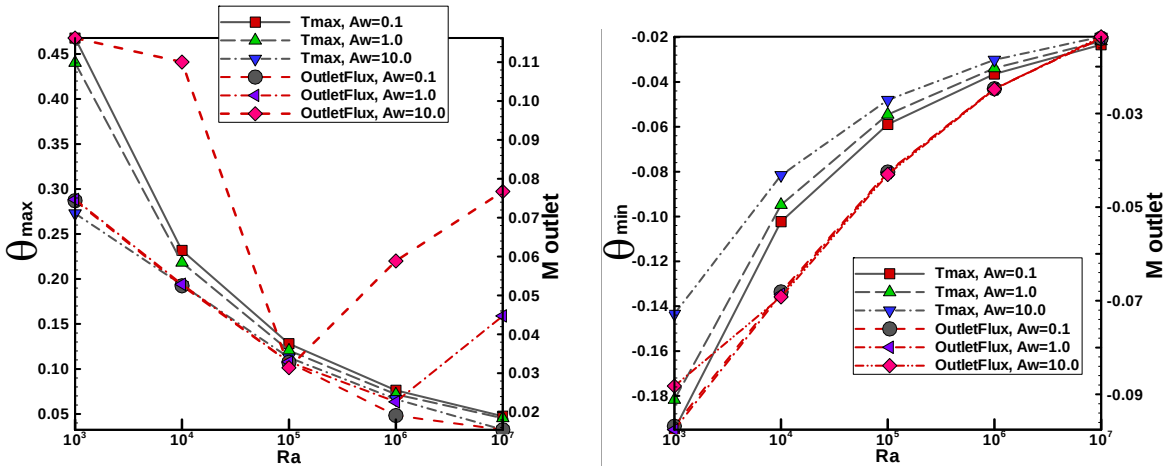

4.1 Heating channel **4.2 Refrigerating channel**

Fig. 4. Extreme temperatures and mass flow rates on outlet in heating/refrigerating channels (C_{OR}=1.0)

3.3 C_{OR} Equals 10.0

When C_{OR} increases up to 10.0, the fluid flow and heat transfer are agitated and enhanced both in heating and refrigerating channels, $\overline{Nu_V}$ equals 4.4 and 4.0 for heat sources and cooling sources respectively. Form that point, we would take it for granted that the heat transfer and fluid flow are the same or similar in both channels. In Figs. 5.1 and 5.2, the macro varieties of extreme temperatures and outflow rates are similar, such as the extreme temperatures and outflow rates decrease along with the increased *Ra* numbers, but there is discrepancy in the values. For the heating channel, highest temperatures range from 0.10 to 1.30, while they are between –0.10 and –0.90 in the refrigerating channel. In fact, the gravitation here should be emphasized. You know, the gravitation acts in the negative direction of Y-axis, then in heating side, the buoyancy force due to the density difference is acting with the

gravitation reversly; on the contrary, in the refrigerating side, the direction of buoyancy force due to the cooling sources is consistent with that of the gravitation, then the opposition and cooperation/combination are in the heating and refrigerating sides respectively. Therefore, airflow in the cooling side becomes easier than in the heating side when both in the same or similar conditions, then the heat dissipation in cooling side becomes easier than in the heating one, which results in the lower extreme temperatures in the cooling side, and higher in the heating one. As for the impaction of wall conduction ratio, trends encountered in Figs. 5.1 and 5.2 are similar to those in Figs. 3.1 or 3.2, and 4.1 or 4.2. Transitions of out flow rates on the outlet in heating side when C_{OR} equals 10.0 also occur in Fig. 5.1, as the *Ra* numbers equal 10^5 and 10^6 for *Aw*=10.0 and *Aw*=1.0 respectively. But the increased breadth of transition reduces from that in Fig. 3.1 to that in Fig. 4.1, and to that in Fig. 5.1. These attribute to the increased heat transfer capacity of heat sources, which make the boundary layer flow approaches to limitation. Out flow rates on the outlet in refrigerating side of varied *Aw* values shown the similar trends start from the lower *Ra* numbers.

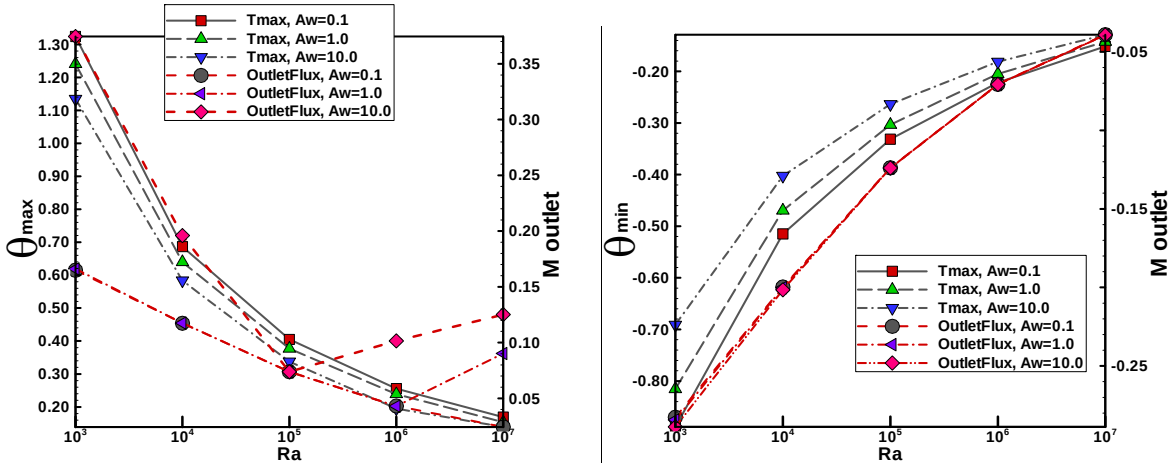

5.1 Heating channel **5.2 Refrigerating channel**

Fig. 5. Extreme temperatures and mass flow rates on outlet in heating/refrigerating channels (C_{OR} =10)

4 CONCLUSION

Natural convection between series of vertical parallel plates with embedded refrigerator/heater was computed in this paper. The critical temperatures (minimum values for refrigerating side, and maximum values for heating side) decrease along with the increased *Ra* numbers. The higher conductivity ratio of walls *Aw*, would reduce the highest or the lowest temperatures in heating/refrigerating channels. Transitions of outlet flow rates occur when *Ra* equals 10^5 and 10^6 for *Aw*=10.0 and *Aw*=1.0 respectively. But the increased breadth of transition decreases from lower C_{OR} values to higher C_{OR} values. The heat dissipation from the heat sources or to the cooling sources is clustered in the center and vicinity of heating/cooling sources, whatever condition being given. Due to the direction of gravitation, the heat transfer and fluid flow show discrepancy in heating and refrigerating channels even though they are in similar conditions. In heating channel, opposition effects lead to heat transfer acutely below the heat

sources; while in refrigerating channel, combination effects lead to heat transfer acutely before the central heat sources. Despite these, the capabilities of heat transfer from two walls to air are similar for the symmetries of heat sources and conductive walls in each channel.

REFERENCES

Astrain D., J. G. Vian, M. Dominguez. 2003. “Increase of COP in the thermoelectric refrigeration by the optimization of heat dissipation,” *Applied Thermal Engineering*, Vol.23, pp. 2183 – 2200.

Chow L. C., S. R. Husain, A. Campo. 1984. “Effects of free convection and axial conduction on forced convection heat transfer inside a vertical channel at low Peclet numbers,” *ASME Journal of Heat Transfer*, Vol.106, pp.297-303.

Desrayaud G., A. Fichera. 2003. “On natural convective heat transfer in vertical channels with a single surface mounted heat flux module,” *ASME Journal of Heat Transfer*, Vol.125, pp.734-739.

Esartea J., G. Minb, D. M. Rowe. 2001. “Modelling heat exchangers for thermoelectric generators,” *Journal of Power sources*, Vol.93, pp.72 – 76.

Hayase T., J. A. C. Humphery, A. R. Grief. 1992. “A consistently formulated QUICK scheme for fast and stable convergence using finite-volume iterative calculation procedures,” *Journal of Computational Physics*, Vol.93, pp.108-118.

Kim S. H., N. K. Anand, L. S. Fletcher. 1991. “Free convection between series of vertical parallel plates with embedded line heat sources,” *ASME Journal of Heat Transfer*, Vol.113, pp.108-115.

Manca O., S. Nardini, V. Naso. 2002. “Effect on natural convection of the distance between an inclined discretely heated plate and a parallel shroud below,” *ASME Journal of Heat Transfer*, Vol.124, pp. 441-451.

Patankar S. V. 1980. *Numerical Heat Transfer and Fluid Flow*, Hemisphere, Washington, D.C.

Rowe D. M., C. M. Bhandari. 1983. *Modern Thermo-electrics*, Holt, Rinehart and Winston, London.

Said S. A. M., R. J. Krane. 1990. “An analytical and experimental investigation of natural convection heat transfer in vertical channels with a single obstruction,” *International Journal of Heat and Mass Transfer*, Vol.33, pp.1121-1134.

Sparrow E. M., M. Faghri. 1980. “Natural convection heat transfer from the upper plate of a collinear, separated pair of vertical plates,” *ASME Journal of Heat Transfer*, Vol.102, pp.623-629.

Suzuki R. O., D. Tanaka. 2003. “Mathematical simulation of thermoelectric power generation with the multi-panels,” *Journal of Power Sources*, Vol.122, pp.201-209.

Vian J. G., D. Astrain, M. Dominguez. 2002. “Numerical modeling and design of a thermoelectric dehumidifier,” *Applied Thermal Engineering*, Vol.22, No.4, pp.407 – 422.

ACKNOWLEDGEMENTS

The authors gratefully acknowledge the financial support of National Natural Science Foundation of China (No. 50408019).